Available online at www.sciencedirect.com
ScienceDirect
Trans. Nonferrous Met. Soc. China 32(2022) 1834−1851
Transactions of Nonferrous Metals Society of China
www.tnmsc.cn

A novel approach for evaluation of load bearing capacity of duplex coatings on aluminum alloy using PLS and SVR models

Farideh DAVOODI[1], Fakhreddin ASHRAFIZADEH[1], Masoud ATAPOUR[1], Reyhaneh RIKHTEHGARAN[2]

1. Department of Materials Engineering, Isfahan University of Technology, Isfahan 84156-83111, Iran;
2. Department of Mathematical Sciences, Isfahan University of Technology, Isfahan 84156-83111, Iran

Received 29 June 2021; accepted 22 December 2021

Abstract: Duplex NiP/TiN coatings consisting of the electroless intermediate layers and the physical vapor deposition (PVD) top layers were fabricated on the AA6061 aluminum alloy in order to enhance the load bearing capacity. The main objective of this study was to model the load bearing based on the thickness, adhesion and elastic modulus of the coatings. For this purpose, partial least square (PLS) and support vector regression (SVR) approaches were employed. The results showed that both models had an acceptable performance; however, the PLS model outperformed SVR. The correlation coefficients between thickness, adhesion and elastic modulus with load bearing were 0.841, 0.8092 and 0.7657, respectively; so, thickness had the greatest effect on the load bearing capacity. The composition and structure of the samples were evaluated using XRD and SEM. The load capacity of the coated samples was also discussed based on the wear and adhesion evaluations. Dry sliding wear tests, under a load of 2 N and a sliding distance of 100 m, demonstrated the complete destruction of the coated specimens with low load capacity. The samples with high load capacity showed not only a superior tribological performance, but also a remarkable adhesion according to the Rockwell superficial hardness test.

Key words: load bearing; aluminum alloys; NiP interlayer; TiN coating; partial least square, support vector regression

1 Introduction

Physical vapor deposition (PVD) coatings have played an important role in improving the wear and thermal resistance, as well as corrosion protection properties [1−5]. However, the problem is that PVD coatings are relatively thin, hard and brittle and, if they are applied on soft metals with low hardness and low elastic modulus, deformation of the substrate could occur under high contact stress, leading to bending, cracking or fracture of the coating [6,7]. This means that the load carrying capacity of such a system is too low for high-stress applications.

The design of duplex systems, using coating technologies to prevent cracking of the coating and to hinder plastic deformation of the substrate, can be regarded as a promising method [8]. For example, the deposition of the electroless nickel interlayer between the PVD top coating and the substrate has been proposed in the literature. For instance, WILSON et al [9] reported that the electroless nickel-phosphorous (NiP) interlayer with a thickness of 24 μm improved the load support and tribological performance of PVD coatings on copper alloys. LIN et al [10] showed that the duplex electroless nickel/CrN/ZrN coatings on ductile iron reduced the friction coefficient and wear rate of the system, in comparison with a single coating. In another attempt, STAIA et al [11] demonstrated that the wear rate of the NiP/DLC coating on Al 2024-T6 was remarkably lower than that in the uncoated aluminum alloy.

Corresponding author: Farideh DAVOODI, E-mail: f.davoodi@ma.iut.ac.ir
DOI: 10.1016/S1003-6326(22)65912-0
1003-6326/© 2022 The Nonferrous Metals Society of China. Published by Elsevier Ltd & Science Press

Coating thickness has been shown to have a strong effect on the load bearing of systems [12], but the required thickness for protecting the substrate from deformation is not often well known. KOMVOPOULOS [13] reported that when a stiff coating system is loaded by a sphere, the coating thickness should be larger than the half-width of the contact area in order to protect the substrate from plastic deformation. Another key factor on the load bearing capacity is the coating−substrate adhesion [14,15], because the first requirement for the use of coating systems in contact conditions and tribology is the strong bonding of deposited coatings to the substrate. Finally, elastic modulus of the coated sample is the other significant influential factor on the load bearing capacity. In a previously published literature [16], the influence of the elastic modulus of polyuria layer on a ceramic coating was investigated. To study the mechanism of flexural strength, the analysis of the load–displacement of the coated ceramic specimens with different elastic moduli of the polyuria coating was carried out. The results confirmed that the higher modulus coating led to more load bearing capacity of the coated sample and its flexural strength. According to YE et al [17], the elastic modulus mismatch between the deposited film and the substrate is one of the key factors determining the performance and load bearing of WC/C coated substrates. The results have also illustrated that the small mismatch of elastic modulus could contribute to the tribological performance of the systems.

Given the effect of thickness, adhesion and elastic modulus on the load bearing, it can be acknowledged that there must be a relationship between these three factors and the measured load bearing; therefore, appropriate methods are needed to develop some mathematical models. One of those good techniques is supervised statistical learning method; this includes a set of predictor variables, X_j, j=1, 2, ⋯, p, and a dependent variable, Y. By this process, Y can be predicted by the proposed model [18].

Over the years, there have been some attempts focusing on the modeling of coating characteristics by statistical learning theories. YAZDI et al [19] estimated the maximum hardness of titanium films based on pressure and temperature conditions by using the artificial neural network. It was observed that the neural network results and experimental data have an excellent agreement with each other. RAFIEERAD et al [20] also proposed the genetic algorithm as an accurate model to predict the hardness and adhesion strength of niobium PVD coatings by using the DC bias, the argon flow rate and DC power. In another work done by CHEN et al [21], a prediction model based on the support vector machine (SVM) was developed for the thickness and microhardness of coatings by considering laser cladding process parameters (27 groups of the experimental data). The correlation coefficient and determination coefficient for the model were greater than 0.9, thus the model had high accuracy.

In this work, 18 specimens of different duplex coatings were prepared in an attempt to present a new method to estimate load bearing. Due to limitations in the coating system, the size of the obtained experimental data was small. To overcome this problem, the resampling techniques and appropriate models with less complexity could be attractive. One of the methods considered for small datasets is the SVM method [22]. One of the most important branches of SVM, based on the statistical learning theory, is support vector regression (SVR), which is good for solving nonlinear regression problems with the minimum structural risk [23]. Partial least squares (PLS) is another statistical regression method presenting the results in the form of formulas; it also has the minimum variance among the estimators considered [24].

No single definition of the load capacity has yet been provided. Tribology test [7], indentation test [12] and scratch test [5,7] are regarded as the most common techniques for assessing the load bearing capacity of the coating system by using the critical load. In the present work, the load bearing capacity of the coated samples, in terms of the thickness, adhesion of the interlayer to the substrate and the elastic modulus, was evaluated using PLS and SVR models. Finally, the wear loss and adhesion of typical coatings of different load bearing capacities were measured experimentally and compared with analytical data.

2 Experimental

2.1 Substrate materials

6061-T6 aluminium alloy with the chemical

composition (wt.%) of 1 Mg, 0.65 Fe, 0.6 Si, 0.35 Cr, 0.2 Cu, 0.2 Zn, 0.15 Mn, 0.13 Ti and balanced Al was used as the substrate material. The samples were cut and mirror polished to a surface roughness of ~ 0.05 μm, then, they were degreased in ethanol and rinsed with deionized water.

2.2 Coating processing

Nickel phosphorous with different thicknesses ranging from 5 to 25 μm was deposited on the aluminum substrates as the intermediate layer; this was followed by TiN coating with the thicknesses of ~2 μm and ~5 μm as the top coating. The nomenclature of the specimens is presented in Table 1. SLOTONIP 70A solution, which is a commercial bath for the electroless process, was purchased from Schlotter Company (Geislingen, Germany).

TiN coatings were deposited over the NiP coated specimens by an industrial cathodic vacuum arc PVD system with a chamber having a volume of 0.86 m^3; it was equipped with Ti target (99.5% purity) and a mixed atmosphere of 99.99% argon and 99.99% nitrogen gases. The process parameters for deposition of NiP and TiN coatings are summarized in Tables 2 and 3, respectively.

2.3 Estimation of load bearing

Load bearing of the alloys was obtained using hardness vs load curves. The curves for some samples with different hardnesses are depicted in Fig. 1. For this purpose, a Vickers microhardness tester, Leitze Wetzlar model, was used at room temperature and the average values of five indentations were reported on each load. Although small loads were employed for hardness measurements, the indentation depth was greater than 1/10 of the total thickness of the coating and the intermediate layer and, accordingly, the hardness reported at each load was influenced by the hardness of the substrate. This dependency was supposed to be similar for all specimens, thus, no significant effect on the calculation of the load bearing.

Table 1 Nomenclature of specimens

Specimen	Substrate	Type of interlayer	Thickness of interlayer/μm	Thickness of TiN/μm
TiN2	Al 6061	−	0	2
TiN5	Al 6061	−	0	5
5L-2	Al 6061	Ni-low phosphorous	5	2
15L-2	Al 6061	Ni-low phosphorous	15	2
25L-2	Al 6061	Ni-low phosphorous	25	2
5M-2	Al 6061	Ni-medium phosphorous	5	2
15M-2	Al 6061	Ni-medium phosphorous	15	2
25M-2	Al 6061	Ni-medium phosphorous	25	2
5H-2	Al 6061	Ni-high phosphorous	5	2
15H-2	Al 6061	Ni-high phosphorous	15	2
25H-2	Al 6061	Ni-high phosphorous	25	2
5L-5	Al 6061	Ni-low phosphorous	5	5
15L-5	Al 6061	Ni-low phosphorous	15	5
25L-5	Al 6061	Ni-low phosphorous	25	5
5M-5	Al 6061	Ni-medium phosphorous	5	5
15M-5	Al 6061	Ni-medium phosphorous	15	5
25M-5	Al 6061	Ni-medium phosphorous	25	5
5H-5	Al 6061	Ni-high phosphorous	5	5
15H-5	Al 6061	Ni-high phosphorous	15	5
25H-5	Al 6061	Ni-high phosphorous	25	5

Table 2 Process parameters for NiP coatings

Process parameter		Value
Process temperature/°C		85−90
Agitation speed/(r·min^{-1})		750
pH	Low phosphorous	5.60±0.05
	Medium phosphorous	4.70±0.05
	High phosphorous	3.60±0.05
Deposition rate/(μm·h^{-1})		18−22

Table 3 Parameters for arc PVD process

Process parameter	value
Chamber pressure before deposition/Pa	0.008
Substrate bias voltage/V	100
Rotational speed of substrate/(r·min^{-1})	10
Temperature during coating process/°C	120±10
Time required to get 1 μm thickness of coating/min	60
Sputtering time/min	20
Arc current/A	120
Distance between sample and target/cm	30

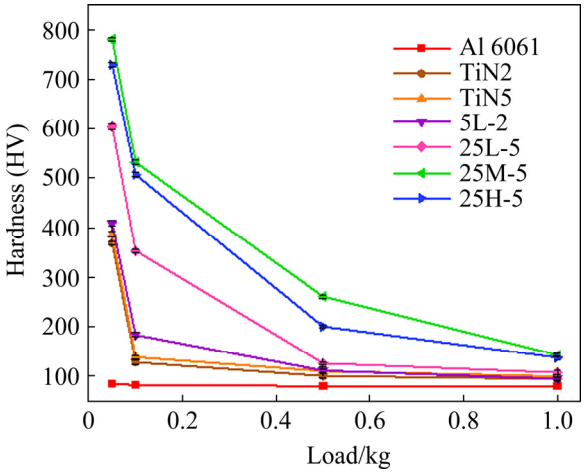

Fig. 1 Curves of hardness vs applied load for specimens

Indentation tests such as microhardness test or Rockwell indentation test are frequently used to determine the static load capacity of a coated system. Figure 2 presents schematically a coated specimen under load during hardness test and the accompanied deformation area. High pressures produced by high normal loads are transmitted to the substrate through the coating, leading to elastic and plastic deformation. By applying the proper intermediate coating, the interfacial stresses could be spread onto the interlayer, thus protecting the substrate from them [25]. It can be said that the obtained hardness relative to the applied load, depends on the load bearing of each sample. In this study, a criterion was defined to estimate the load bearing capacity in order to compare the specimens, numerically. Load bearing could be assumed as a combination of the applied load and specimen hardness; it was measured as the area under "hardness vs load" curves for each specimen.

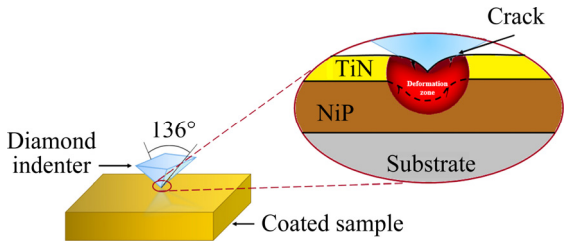

Fig. 2 Schematic diagram of microhardness test showing deformation zone below indenter

Formulation of load bearing (Y) was carried out based on three variables: thickness (X_1), adhesion (X_2) and elastic modulus (X_3). Total thickness of the intermediate layer and the top coating, the adhesion of the intermediate layer to the substrate and the elastic modulus of the duplex coating were considered as X_1, X_2 and X_3 variables, respectively. The total thickness of the cross-section was obtained by adjusting the parameters of the coating processes; it was measured using scanning electron microscopy (SEM) images (model: Philips XL30).

In addition to the thickness and the type of electroless layer, there are more important factors affecting the adhesion of electroless layer on aluminum substrate such as heat treatment and zincating treatment. Difference in adhesion values due to the heat treatment has been reported by many authors. BOUAZIZ et al [26] and, RAMALHO and MIRANDA et al [27] have shown that with increasing temperature, a diffusion layer between the substrate (especially light substrates like aluminum and titanium) and the electroless coating is formed, as a result, hardness and adhesion strength increase. SUDAGAR et al [28] and HINO et al [29] have demonstrated that the double zincate layer led to stronger metallurgical bonds between the coating and the substrate than that of single

zincate layer during electroless process. For modeling of the problem, layers with different adhesion values were needed, and we found that with the operation presented in Table 4, a specific adhesion could be obtained for each specimen. By definition, adhesion is the bonding strength between the substrate and the coating in contact at the interface, although the film can be single layer or multilayer. In the present research, TiN was selected as the top layer, produced by PVD process from a vapor source. The adhesion of this top coating is much higher than that of the NiP coating to the substrate and no de-bonding of TiN occurred during the adhesion tests. Therefore, the adhesion between the layers was not considered in the models, instead, the focus was on the adhesion of NiP to the substrate.

The adhesion strength at the substrate−NiP interface was measured using the pull-off adhesion test inspired by ASTM C 633. A Hounsfield H25KS tension testing machine at 1 mm/min of crosshead speed was then employed to apply the tensile load. In this method, the NiP-coated sample was glued by 3M Scotch Weld-2214 epoxy adhesive to a counterpart with a diameter of 12 mm that was grit blasted. After mounting in the self-aligning device at 121 °C for 40 min, the adhesion strength was tested in the machine. The adhesion strength was obtained by dividing the failure load to the cross-sectional area of the specimen. The test was repeated three times on each coating, and the results were averaged. The adhesion test set-up is schematically depicted in Fig. 3.

Nano-indentation tests were then conducted with a diamond indenter under a maximum load of ~ 10 mN to determine the elastic modulus. In order to eliminate the substrate effect, the indentation depth was kept below 1/10 of the total thickness of the interlayer and the top coating [30]. The tests were repeated three times and the average of the reduced elastic modulus (E_r) was calculated for each specimen. When E_r is derived from the nano-indentation test, the elastic modulus of the duplex coating (E) can be determined from Eq. (1):

$$\frac{1}{E_r}=\frac{1-\nu_i^2}{E_i}+\frac{1-\nu^2}{E} \tag{1}$$

where E_i and ν_i are the elastic modulus and Poisson's ratio of the indenter, respectively, and ν is the Poisson's ratio corresponding to the duplex coating. Also, ν can be obtained from Eq. (2) [31]:

$$\nu=\nu_m V_m+\nu_c V_c \tag{2}$$

where ν_m and ν_c refer to the Poisson's ratios of the metallic (NiP) and ceramic coatings (TiN), respectively. Based on the previous reports, ν_m is ~0.3 [11] and ν_c is ~0.25 [32]. V_m and V_c indicate the volumetric ratios of the metal and ceramic coatings, respectively.

The input and output values for the specimens are presented in Table 5. Adhesion and elastic modulus values were acquired by using the tests, and the load bearing values of different specimens are also shown in the bar plot represented in Fig. 4.

Table 4 Effective operations applied to obtaining different values of adhesion between NiP and substrate

Type of interlayer	Thickness of interlayer/μm	Heat treatment (400 °C for 1 h)	Very low zincating treatment (1 s)	Single zincating process (5 s)	Double zincating process (15 s + 20 s)
Ni-low phosphorous	5	✓	✓		
Ni-low phosphorous	15	✓		✓	
Ni-low phosphorous	25			✓	
Ni-medium phosphorous	5	✓		✓	
Ni-medium phosphorous	15				✓
Ni-medium phosphorous	25	✓			✓
Ni-high phosphorous	5			✓	
Ni-high phosphorous	15	✓			✓
Ni-high phosphorous	25				✓

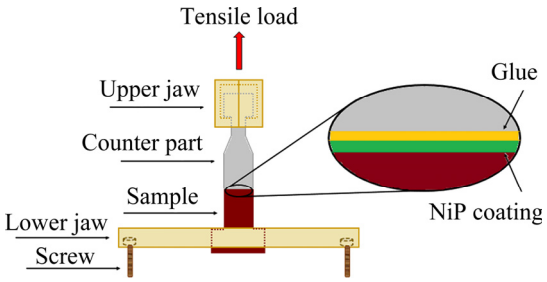

Fig. 3 Schematic diagram of pull-off adhesion test

Table 5 Input and output values of specimens

Specimen	Input			Output, Y/ ($kg^2 \cdot mm^{-2}$)
	X_1/μm	X_2/MPa	X_3/GPa	
5L-2	7	7.8	280.5	125.31
15L-2	17	15.27	281.2	139.265
25L-2	27	13.8	310.3	225.245
5M-2	7	14.32	268.2	119.215
15M-2	17	20.4	290.2	191.445
25M-2	27	24.33	301.4	228.885
5H-2	7	10.83	241.2	122.93
15H-2	17	21.76	278.4	196.755
25H-2	27	18.57	295.6	221.52
5L-5	10	7.8	276.9	126.46
15L-5	20	15.27	287.8	156.2
25L-5	30	13.8	306.2	178.305
5M-5	10	14.32	289.6	164.16
15M-5	20	20.4	297.1	208.41
25M-5	30	24.33	347.2	292.5
5H-5	10	10.83	248.3	131.355
15H-5	20	21.76	279.5	241.165
25H-5	30	18.57	296.7	257.02

3 Modeling of load bearing

3.1 Theory of PLS and SVR

PLS is a multivariate technique for path modeling latent variables by projecting the predictor and response variables to a new space, then it can predict dependent variables based on the independent variables [33]. The details of the PLS method can be found elsewhere [34].

SVR is applied to solving the regression problems. For this purpose, a training data set T= [(x_1, y_1), ⋯, (x_l, y_l)], where x_i, y_i and l denote the input values, output values and the size of dataset,

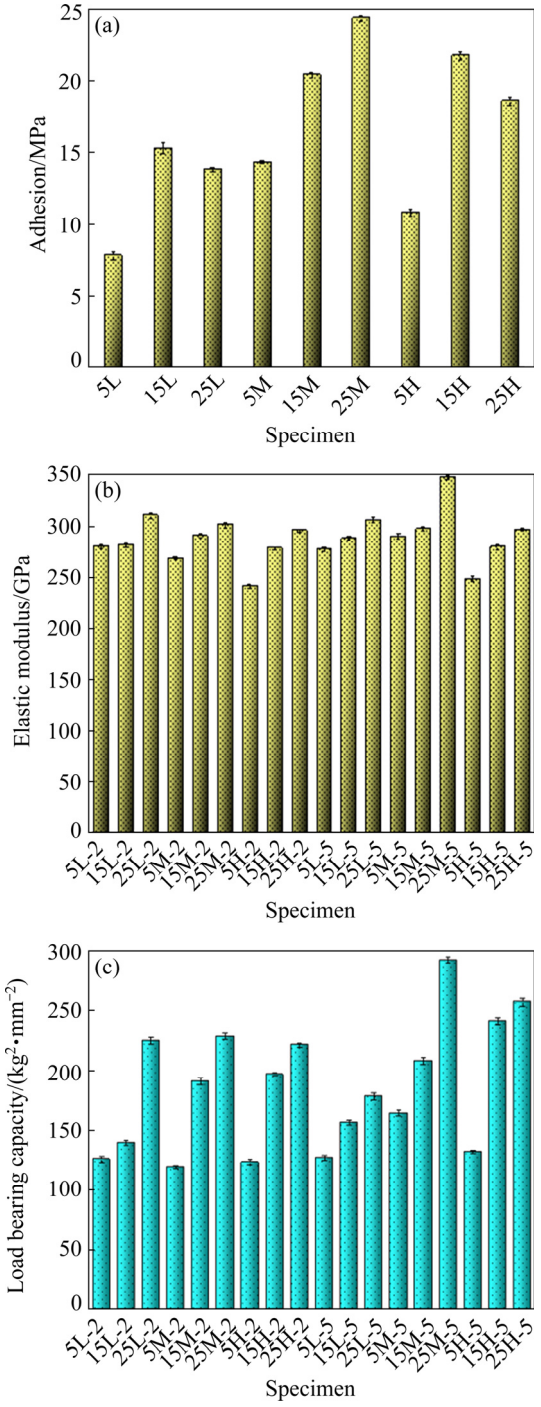

Fig. 4 Adhesion (a), elastic modulus (b) and load bearing capacity (c) of specimens

respectively, must be considered, and a linear regression function $f(x)$ is also defined in order to minimize the structural risk $R[f]$. The relevant relationships are shown in Eqs. (3) and (4):

$$f(x)=\boldsymbol{w}\cdot\varphi(x)+b,\ \boldsymbol{w}\in\mathbf{R}^n,\ b\in\mathbf{R} \tag{3}$$

$$R[f]=\int L(y,f(x))\mathrm{d}p(x,y) \tag{4}$$

where $\boldsymbol{w}$ is the weight vector, $\varphi(x)$ is a function for

the non-linear mapping of the input data to the higher dimensional space, **R** is the real number, $R[f]$ is the regularized risk function or structural risk, $p(x, y)$ is the joint probability function of x and y, b is a constant, and L is the loss function, as shown in Eq. (5):

$$L(y, f(x)) = \begin{cases} |f(x) - y| - \varepsilon, \text{ if } |f(x) - y| \geq \varepsilon \\ 0, \text{ otherwise} \end{cases} \quad (5)$$

where ε is a given positive number representing the distance around the regression function $f(x)$.

The details of the SVR method can be found elsewhere [23].

Usually, in order to make prediction based on the new data in the learning models, the train-test split is a good procedure for performance estimation. Training data are a dataset used for training the algorithm and fitting the model. Testing dataset is used to provide an evaluation of the obtained model from the training dataset. The train-test split procedure is good for a very large dataset; however, in this work, the dataset acquired from experiments represented a small sample size. To cope with this problem, resampling methods like k-fold cross validation method was employed as an appropriate strategy [35]. Accordingly, all data were selected for both training and validation sets. The available data were partitioned into six equal groups. A fold was then considered as the validation set and other $k-1$ folds were assigned to the training set. The accuracy of the models was evaluated by all six cases of cross validation. The statistical criteria were defined as the average of the obtained criteria from each partition.

Double interaction terms were also added to the regression models to better understand the relationships among the variables under study, and the selection of the variables was done using backward stepwise selection. All modelings were done using Matlab 2018a.

3.2 Performance comparison

The coefficient of determination (R^2), the adjusted determination coefficient (R^2_{adj}), the root mean square error (RMSE), Akaike information criterion (AIC) and Bayesian information criterion (BIC) were used as an assessment index system to measure the efficiency of the PLS and SVR models. R^2 is the proportion of the variance of a dependent variable as explained by the fitted model, R^2_{adj} is a modified version of R^2 that accounts for the predictors which are not significant in a regression model, RMSE is an ideal index used to evaluate the error of a model, and AIC and BIC help to obtain the best model that fits the data. The mentioned statistical criteria are defined as

$$R^2 = 1 - \frac{\sum_{i=1}^{n}(y_i - \hat{y}_i)^2}{\sum_{i=1}^{n}(y_i - \bar{y})^2} \quad (6)$$

$$R^2_{adj} = 1 - \frac{(1 - R^2)(n-1)}{n - P - 1} \quad (7)$$

$$\text{RMSE} = \sqrt{\frac{1}{n}\sum_{i=1}^{n}(y_i - \hat{y}_i)^2} \quad (8)$$

$$\text{AIC} = 2K - 2\ln L \quad (9)$$

$$\text{BIC} = K\ln n - 2\ln L \quad (10)$$

where y_i is the observed output data, $\hat{y}_i$ is the estimated value, $\bar{y}$ is the mean values in the dataset, n is the total sample size, P is the number of predictors, K is the number of the parameters of the models, and L is the likelihood function.

4 Experimental evaluations

For experimental evaluations and qualitative comparison of the load bearing capacities, some samples including single and duplex coatings with different values of load bearing (low, medium and high load capacity) were considered. For this purpose, TiN2, TiN5, 5L-2, 25L-5, 25H-5 and 25M-5 with the load bearing values of 106.9, 115.4, 125.3, 178.3, 257.0 and 292.5 kg^2/mm^2, respectively, were selected.

4.1 Characterization

Microstructural examination of the cross-sections was carried out by SEM. To study the phase analysis of the specimens, an X-ray diffractometer (XRD, Philips XPERT-MPD) was utilized. The X-ray was generated by a Cu target that was operated at 40 kV and 30 mA, in a scanning angular range of 20°−100°, with the step size of 0.05° and counting time per step of 1 s.

4.2 Wear tests

To compare the wear behavior and load bearing of the coatings, the coated samples were examined using a ball on disc tribometer. Schematic diagram of the experimental set-up for the wear

tests is shown in Fig. 5. The coated alloys were prepared in the disc shape with dimensions of 50 mm (diameter) × 5 mm (thickness); as a counter body, a zirconia ball with the hardness of 13.5 GPa and a diameter of 10 mm was used. The wear experiments were performed at a normal load of 2 N, a sliding velocity of 0.06 m/s and a sliding distance of 100 m by pressing zirconia balls towards the rotating disc specimens. Three wear tests were carried out for each coated specimen at 25 °C under ambient humidity to ensure the repeatability of the tests. After test, the wear tracks were studied by using SEM and energy dispersive X-ray spectroscopy (EDS).

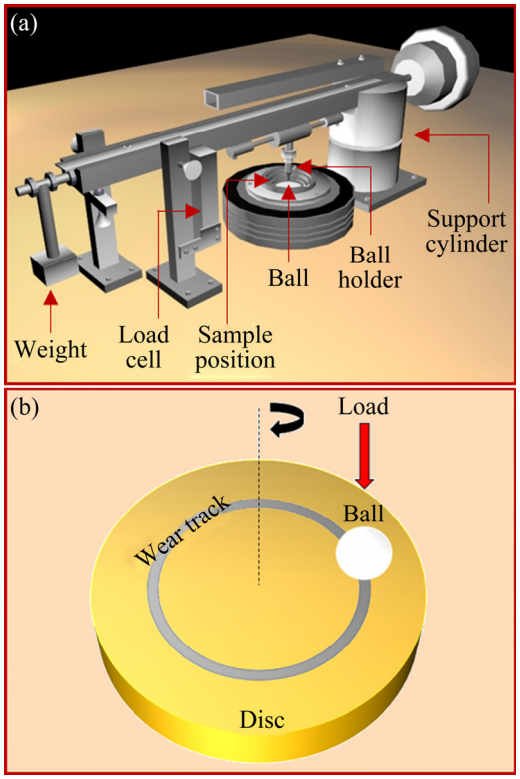

Fig. 5 Schematic diagrams of ball-on-disc wear apparatus (a) and disc sample and ball (b)

4.3 Adhesion test

A Rockwell superficial hardness test was then performed according to ASTM E18 for the qualitative evaluation of the coatings adhesion. In this regard, a universal hardness tester device equipped with a Rockwell C tip having a radius of 200 μm was utilized. A load of 45 kg was applied to producing indentations on each surface. An optical microscope (Nikon EPISHOT 300 microscope) was then employed to examine the images. The obtained micrographs were scaled by the ImageJ software.

5 Results and discussion

5.1 PLS and SVR models

The results obtained by PLS and SVR models for the prediction of load bearing are shown in Fig. 6. In these plots, high-precision models show more points with less scattering near the bisector line. Given the distribution of points for both models, it could be said that the predicted values of the models and the values obtained from experiments were close to each other; both models indicated acceptable accuracy. To compare the model performance, R^2, R^2_{adj}, RMSE, AIC and BIC were calculated for the training and validation sets, as presented in Table 6. For the PLS model, R^2 and R^2_{adj} of the training set were lower than those obtained from the SVR model; however, for the validation set, the values of these statistical criteria in the PLS model were higher. Nevertheless, the less influence of R^2 on detecting generalization issues and performance comparison of models has

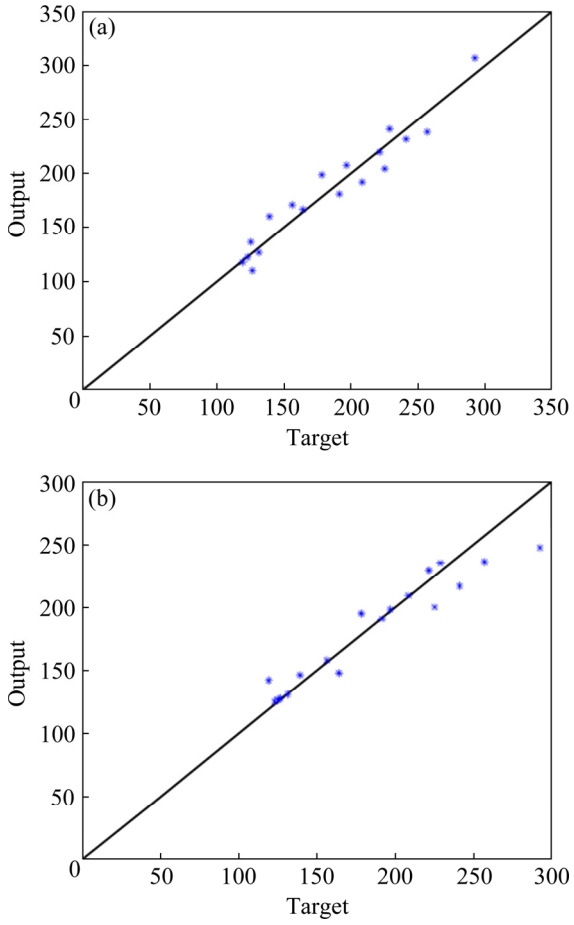

Fig. 6 Scatter plots of PLS (a) and SVR (b) models for experimental (target) and predicted (output) values (after 6-fold cross validation)

Table 6 Comparison of statistical criteria for different models

Index	PLS		SVR	
	Training set	Validation set	Training set	Validation set
R^2	0.945	0.932	0.956	0.796
R^2_{adj}	0.941	0.864	0.953	0.592
RMSE	11.715	28.905	13.588	32.73
AIC	2106.1	2862.2	4219.9	3586.7
BIC	2112	2863.3	4225.8	3587.8

been expressed [23]. RMSE, AIC and BIC must include the lowest values to obtain the best model. So, the highest accuracy based on RMSE was obtained for the PLS model. On the other hand, the PLS model had lower AIC and BIC, therefore, it could better fit the experimental data in comparison to SVR. By comparing the performance of the models, it could be said that both models were acceptable, but the PLS model was superior to the SVR method.

PLS regression of the response variable (Y), by considering double interactions and detecting the non-significant terms, led to Eq. (11):

$$Y = 5016 + 76.6119X_1 + 90.6119X_2 - 44.3635X_3 + 0.2501X_1^2 + 0.0971X_3^2 + 0.5685X_1X_2 - 0.3354X_1X_3 - 0.3186X_2X_3 \quad (11)$$

Selecting variables using the backward procedure in the SVR method created the most accuracy for a model based on four variables: X_1, X_2, X_3 and X_2X_3.

The coefficients of correlation between thickness (X_1), adhesion (X_2) and elastic modulus (X_3) with load bearing (Y) were 0.841, 0.8092 and 0.7657, respectively. In fact, all inputs had a high effect on the load capacity.

The load bearing which was measured as the area under hardness vs load curves, was achieved by averaging repetitions (m=5) of the experiment at each level of independent variables. This average, $\overline{Y}_i = \frac{1}{m}\sum_{j=1}^{m} Y_{ij}$ (that is the measured load bearing capacity) was recorded for the ith pattern of independent variables and considered as the response variable for this pattern. Then, a model was fitted based on the observed $\overline{Y}_i$ (i=1, ⋯, n) and independent variables. Then, based on this fitted model, a response corresponding to the ith pattern of independent variables can be predicted and showed this prediction by $\hat{Y}_i = X_i'\hat{\beta}$ (that is the calculated load bearing capacity by model), where $\boldsymbol{X}_i'$ and $\hat{\beta}$ are, respectively, p dimensional vectors of independent variables' observations and the estimated regression coefficients. This model is useful for inferring about the effects of covariates on the response variable and also for the predication of the response for new cases. To compare the accuracy of $\overline{Y}_i$ and $\hat{Y}_i$ in predicting the new response (Y_i^*), Eqs. (12) and (13) are used:

$$E[\overline{Y}_i - Y_i^*]^2 = E[\overline{Y}_i - \mu_i]^2 + E[\mu_i - Y_i^*]^2 - 2E[(\overline{Y}_i - \mu_i)(\mu_i - Y_i^*)] = \mathrm{Var}(\overline{Y}_i) + \mathrm{Var}(Y_i^*) = \frac{\sigma^2}{m} + \sigma^2 = \sigma^2\left[1 + \frac{1}{m}\right] \quad (12)$$

where μ_i and σ^2 are, respectively, the expectation and the variance of a response with the ith patterns of independent variables, and

$$E[\hat{Y}_i - Y_i^*]^2 = E[\hat{Y}_i - \mu_i]^2 + E[\mu_i - Y_i^*]^2 - 2E[(\hat{Y}_i - \mu_i)(\mu_i - Y_i^*)] = \mathrm{Var}(\hat{Y}_i) + \mathrm{Var}(Y_i^*) = \mathrm{Var}(\boldsymbol{X}_i'\hat{\beta}) + \sigma^2 = \boldsymbol{X}_i'\mathrm{Var}(\hat{\beta})\boldsymbol{X}_i + \sigma^2 = \sigma^2[1 + \boldsymbol{X}_i'(\boldsymbol{X}'\boldsymbol{X})^{-1}\boldsymbol{X}_i] \quad (13)$$

where $\boldsymbol{X}$ is the $n\times p$ design matrix including all observations for independent variables.

It is seen that when $E[\overline{Y}_i - Y_i^*]^2 < E[\hat{Y}_i - Y_i^*]^2$, the accuracy of $\overline{Y}_i$ in predicting Y_i^* is more than $\hat{Y}_i$, and this depends on the number of repeated measurements (m) and also on the design matrix. To estimate $E[\hat{Y}_i - Y_i^*]^2$ and $E[\overline{Y}_i - Y_i^*]^2$, σ can be replaced by RMSE and then depending on the required pattern of independent variables, these quantities can be computed. Since there are the limitations on the number of repeated measurements, and since there are informative independent variables, the accuracy of $\hat{Y}_i$ is expected to be more than the accuracy of $\overline{Y}_i$.

Using PLS has advantages in comparison to the multivariate multiple regression models usually used for modeling multiple dependent variables, since PLS can handle multicollinearity [36]. Also, the PLS has advantages in comparison to the principal components regression models usually used in the case of having many correlated covariates which focuses on variance while reducing dimensionality instead of the covariance used in the PLS [37]. Moreover, in principal

component regression, the dependent variable is not taken into account when the components are created.

In PLS model, data should be complete and the sample size must be adequate. The standard error size of the estimate is important in the proposed model. The large standard errors are a sign of inadequate sample size [38]. Acceptable errors in the proposed model for load bearing capacity indicated the appropriate sample size in the PLS method.

One of the specific features of PVD coatings is the presence of high residual stress [39]. There are two main sources of residual stress in PVD coatings: thermal stress and intrinsic stress. Thermal stress arises from the mismatched thermal expansion coefficient between the film and substrate during the cooling period after the deposition, and the intrinsic stress is generated in the growth stage [3]. High residual stress can lead to various defects such as cracking, delamination [15], and substrate deformation [17], resulting in the reduced load bearing capacity of the coatings. Increasing the residual tensile stress and defect exerts an undesirable effect on adhesion performance which in turn decreases the load bearing capacity [40]. Using an appropriate interlayer is useful for reducing the residual stress between the top coating and the substrate, thereby, enhancing their bonding strength [4]. It has been reported that the films with many defects lead to reducing in load bearing capacity and the deformation of the substrate; so in this case, the coating is easy to peel off from the substrate [41]. The highest correlation or the strongest linear relationship was found between thickness and load bearing. Thick PVD coatings (>10 μm) may be inefficient because of the more residual stress. On the other hand, although thin layers contain less residual stress and defect, they could not be supported by the underlying metal, properly. If high thickness is provided by the middle layer, a high load bearing can be obtained. It was evident that in coated system with high thickness, better mechanical properties and strong load bearing capacity could be obtained [25]. In a previous study [14], TiN coatings, because of the low thickness, showed a low load capacity; however, they had good adhesion to the aluminum substrate. Without the intermediate layer, the aluminum substrate is rather soft, it is deformed easily and shear fracture occurs near or at the interface. The adhesion of the coating to the substrate and film toughness can control this type of fracture. A good support interlayer not only provides sufficient adhesion, but also improves the mechanical properties and load bearing capacity, inducing a strengthening effect.

5.2 Microstructure

Figure 7 presents the XRD patterns considered to evaluate the crystalline structures of the coated aluminum alloys. There are Ni and TiN diffraction peaks in the XRD patterns for all specimens. The XRD patterns are similar to those in the NiP/TiN coatings deposited on other substrates [42]. In Specimens 5L-2 and 25M-5, due to heat treatment at 400 °C, some peaks appeared from Ni_3P phase at 2θ of 40°−50° [30]; during annealing, the partial transformation of the NiP interlayer to the crystalline phases happened. Aluminum peaks were observed in all specimens related to the penetration of the X-ray into the thin coatings. Because of the low thickness of TiN2, the intensity of Al peaks was at the highest value.

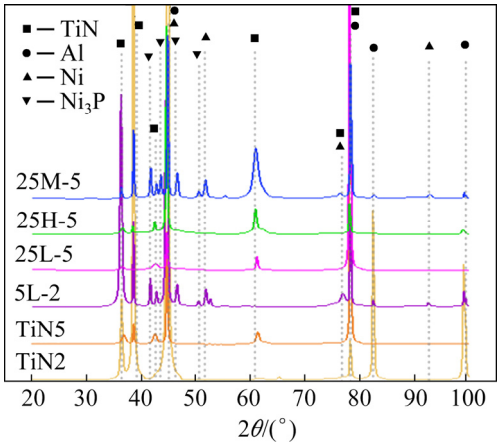

Fig. 7 XRD patterns of coated specimens

During heat treatment of the NiP coatings, diffusion occurs at the interface leading to improved adhesion of the coating. LIEW et al [43] have found that the precipitation of Ni_3P compound and segregation of phosphorous at the grain boundaries during the heat treatment of NiP coatings, lead to improved friction and wear performance. Also, the dissimilar phase boundaries help stopping the movement of dislocations, followed by more hardness of the coating [44]. Increasing the hardness due to the Ni_3P

precipitation, contributes to high load bearing of the coated substrate and improves the wear behavior. However, wrong heat treatment procedure or inadequate zincating treatment might cause a reduction in coating adhesion, thus, undesirable effect on load bearing capacity.

SEM cross-sectional images of TiN2, TiN5, 5L-2, 25L-5, 25H-5 and 25M-5 are presented in Figs. 8(a−f), respectively. The TiN coatings had non-uniform thickness with more defects, in comparison with the NiP, which could be due to the relatively low temperature of the process [45]; in contrast, NiP coatings had a dense and continuous structure in all duplex coatings. Neither sign of poor adhesion of the NiP coatings to the substrate was seen in SEM images for 25L-5 and 5L-2, nor there was pronounced delamination at the interface.

5.3 Wear assessment

Tribological tests are very common in qualitative evaluation of the load bearing capacity of the coating systems. The coefficient of friction (COF) and SEM−EDS analysis of the worn surfaces for various specimens at a load of 2 N and for 100 m sliding distance can be seen in Figs. 9 and 10, respectively. Friction coefficient of the bare aluminum remained almost fixed at an average value of 0.7 (Fig. 9(a)). It was similar to the previous reports in regard to the friction coefficient of Al 6061, which was in the range of 0.75−0.85 against the AISI 52100 steel ball [46] and ~0.65 against an AISI 4140 steel counterface [47]. The fluctuation in the friction trace with the sliding distance could be due to subjecting aluminum to the stick-slip phenomenon. The width of the wear track of Al 6061 was as high as ~1500 μm, reflecting the contact area between zirconia ball and the test specimen (Fig. 10(a)). Plowing lines on the worn surface indicated that the plowing mechanism played an important role in the wear mechanism. Along the sliding distance, the temperature at the contact interface is increased and this could cause the excessive plastic flow [48].

TiN2 and TiN5, as depicted in Figs. 9(b, c), revealed large variations after about 20 and 48 m of sliding, respectively; these were followed by a remarkable rise to around 0.65−0.8, near the COF of the base metal. Observation of the tribological behavior of the TiN coatings and the faster increase in the friction coefficient for TiN2 revealed the

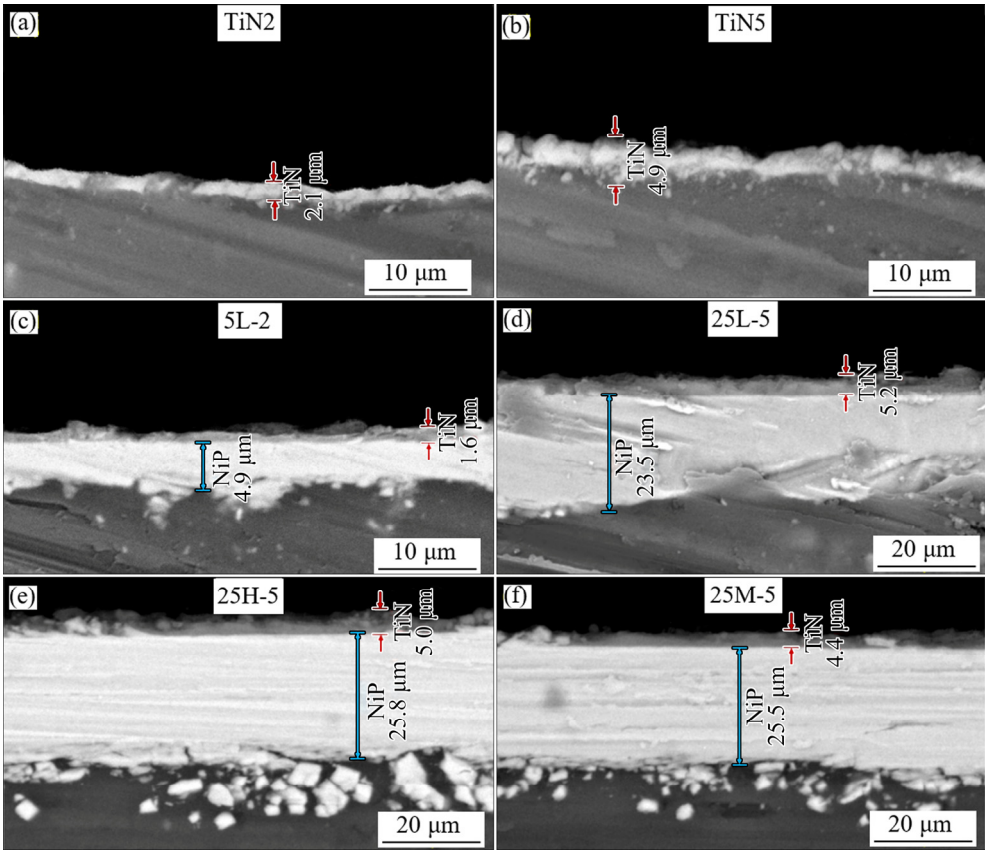

Fig. 8 SEM cross-sectional images of coated specimens

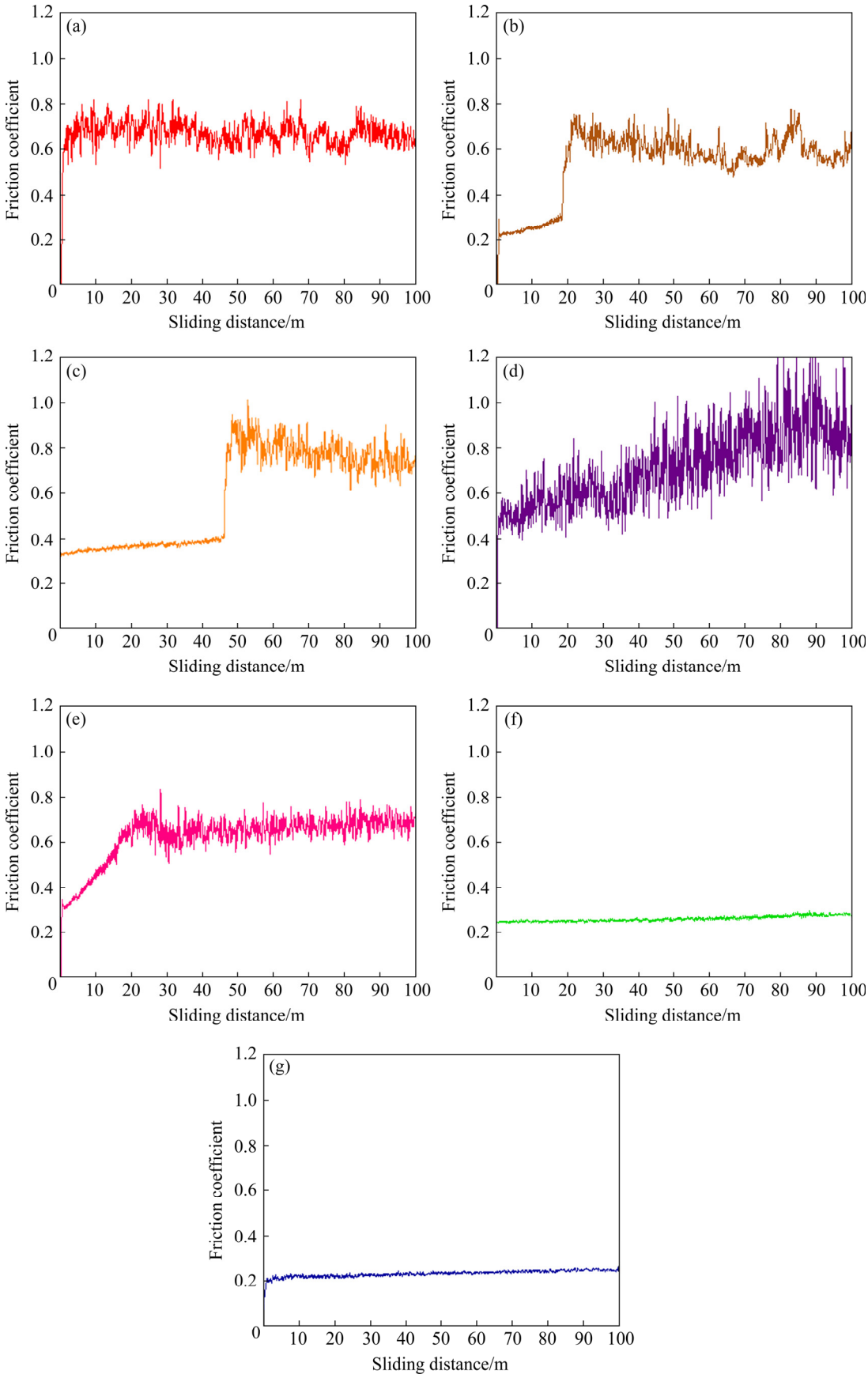

Fig. 9 Friction coefficient evaluation of specimens: (a) Al 6061; (b) TiN2; (c) TiN5; (d) 5L-2; (e) 25L-5; (f) 25H-5; (g) 25M-5

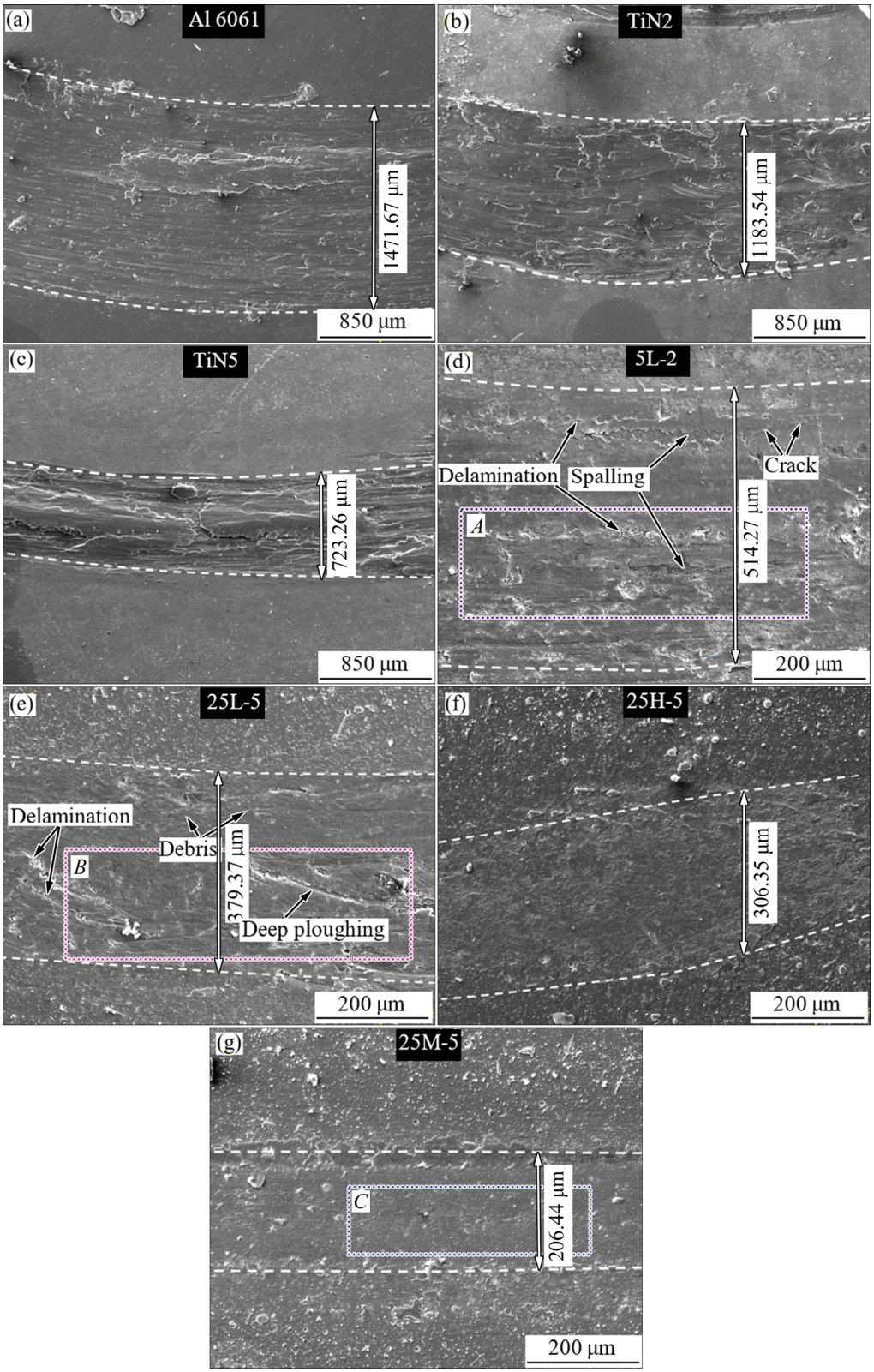

Fig. 10 Wear track morphologies of specimens

lower load carrying capacity of TiN2 as compared to TiN5. After the failure of TiN5, COF began with a value of ~0.8 and ended with a value of ~0.7. Because of the heat generated at the interface during sliding, some debris could be oxidized and transferred to the counterface; a mechanically mixed layer (MML) is formed on the worn surface, leading to the reduction of the COF [49]. Due to the

early failure of TiN2, the substrate was further exposed to wear and the width of the wear track after 100 m sliding was about 450 μm more than that of TiN5; however, the worn surface of both specimens could be described by the formation of deep and long furrows; it was dominated by the abrasive and ploughing wear (Figs. 10(b, c)).

For 5L-2, as shown in Fig. 9(d), the COF had considerably more variations when compared to other specimens, which began from ~0.45 and ended to ~1. This trend might be attributed to the very weak bonding and the poor adhesion between the substrate and the NiP interlayer. Also, fluctuation in the form of sharp peaks was seen, especially in the last 50 m. The width of the wear track was around 515 μm with cracks on it (Fig. 10(d)). The presence of pores could lead to the crack nucleation. Growth and propagation of cracks led to considerable delamination, spallation and high wear rate for this specimen. The analysis of the interface failure mode is useful for estimating the load carrying capacity, in a qualitative manner [17]. EDS analysis relevant to the Region *A* for worn surface of 5L-2 (Fig. 11(a)) also demonstrated the noticeable presence of Zr and O elements, thereby indicating the occurrence of oxidation and the adhesive wear mode. On the other hand, the existence of the Al peak confirmed the failure of the top coating and interlayer in some parts of the surface.

Figure 9(e) illustrates the friction behavior of 25L-5. COF was increased from 0.3 to 0.7 in the first 20 m and then remained unchanged. Wear track morphology, as shown in Fig. 10(e), included debris, delamination and deep ploughing with a width of ~380 μm. The motion and entrapment of the agglomerated wear debris during sliding could cause fluctuation in the friction trace, resulting in the three-body abrasive wear [48]. Considerable quantities of Ni on the worn surface (Fig. 11(b)) belonging to the Region *B* could indicate the failure and delamination of the TiN coating. Better tribological performance of 25L-5 rather than 5L-2 could reflect more load capacity of 25L-5. Higher thickness and improved adhesion strength could contribute to the wear resistance of 25L-5. In the case of 25H-5 and 25M-5, COF was below 0.3 during sliding (Figs. 9(f, g)), and the wear tracks were approximately smooth, with a width of around 300 and 200 μm, respectively (Figs. 10(f, g)). The

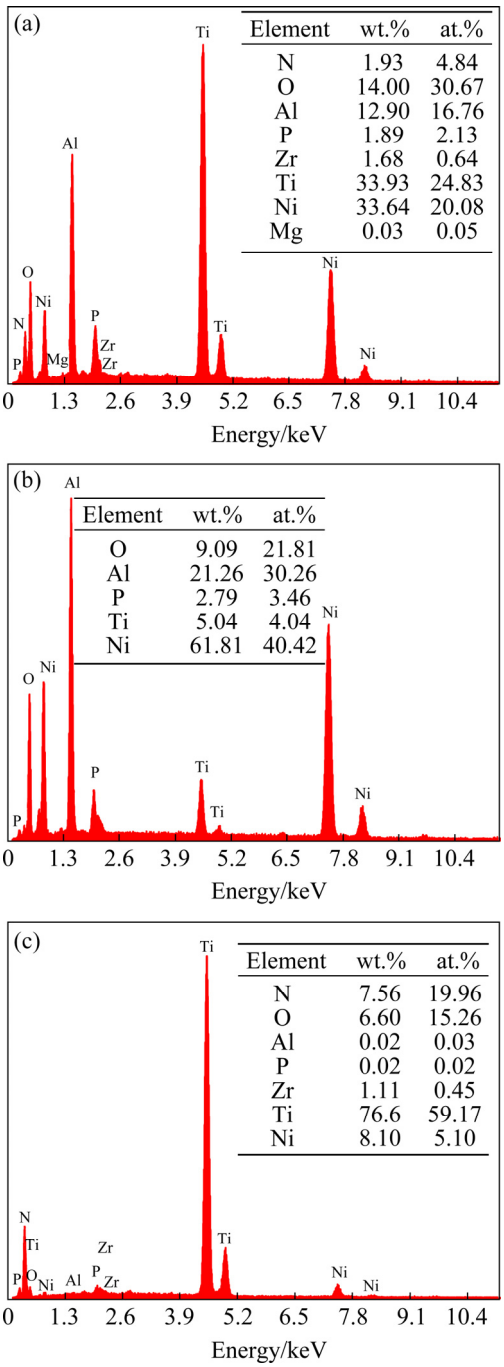

Fig. 11 EDS spectra of Areas *A* (a), *B* (b) and *C* (c) in Fig. 10 on worn surfaces

high amount of Ti element, according to the EDS results (Fig. 11(c)), which was relevant to the Region *C*, indicated that the top coating remained almost intact. Unlike a previous study [50] that the NiP coating with a low amount of phosphorus showed higher wear resistance in comparison to the medium or high phosphorus, in our evaluations, the wear resistance of 25H-5 and 25M-5 was much higher than that of 25L-5, This effect could be

attributed to the better adhesion of the interlayer to the substrate by double zincate treatment [29,51]. Regarding 25M-5, the creation of a homogeneous structure, because of the double zincate processing and heat treatment, resulted in further adhesion strength. The higher wear resistance and load bearing capacity of this specimen are in agreement with previous reports [27,52].

5.4 Adhesion of coatings

Indentation test is one of the common techniques used for the adhesion evaluation of the coatings; the comparison criterion is the size of the damaged area during the test [53]. Optical micrographs of the coated alloys after adhesion tests are shown in Fig. 12. For TiN2, some spherical cracks and spallation were observed (Fig. 12(a)). Delamination of the coating around the indent could be relevant to the brittle nature and poor load capacity of this coating system. Micro indentation enables a qualitative estimation of the cracking behavior; low strength coatings contain more and longer cracks during indentation, whereas well adherent coatings show higher resistance to deformation [54]. For TiN5 (Fig. 12(b)), no spallation was observed, but many circumferential cracks were created during the test. Load bearing capacity of the coatings could be judged from the radial and spherical cracks and the delamination after indentation. It can be seen from Fig. 12(c) that there were a significant number of radial and spherical cracks confirming the weak interfacial

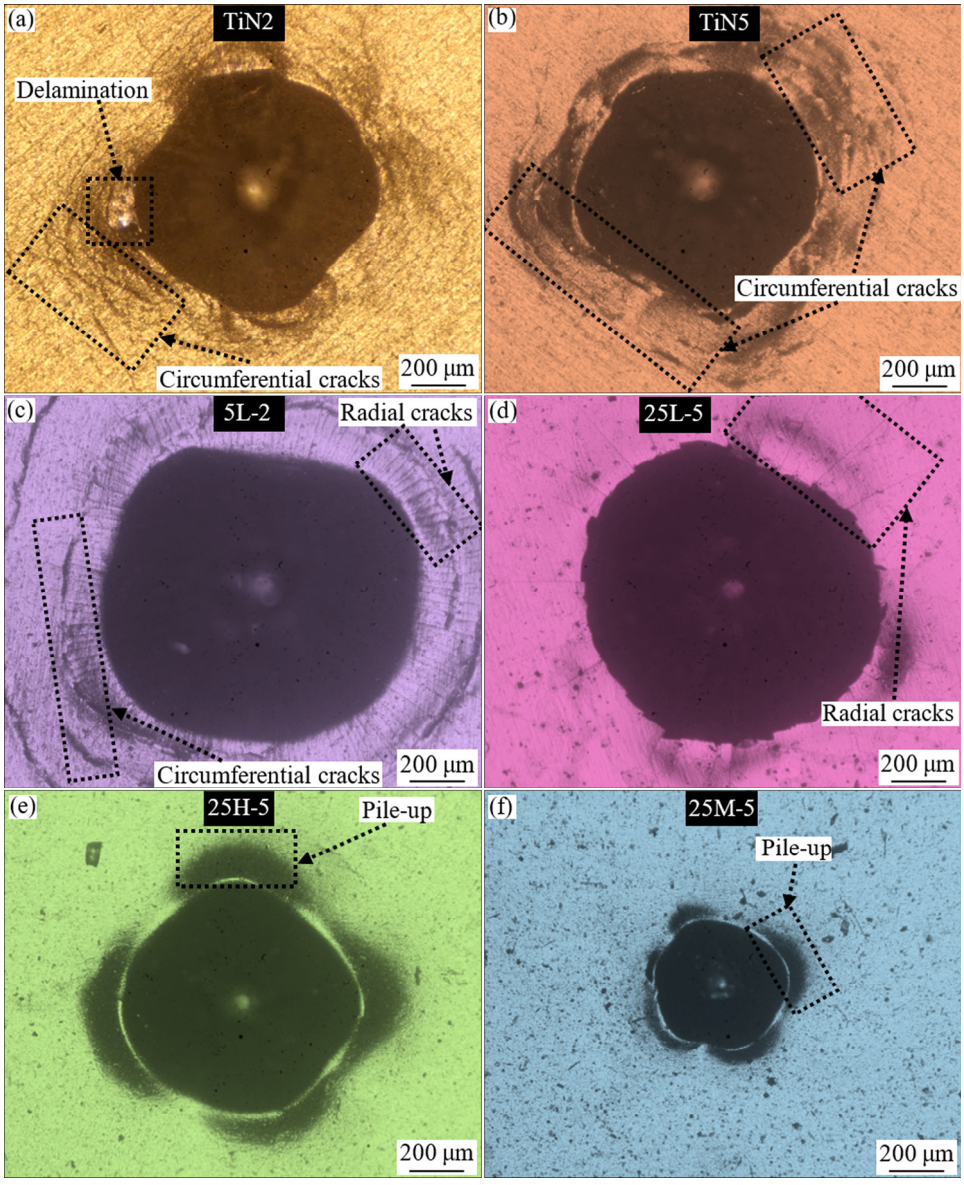

Fig. 12 Rockwell indentation of coated specimens under load of 45 kg

bonds. The very poor adhesion of the interlayer to the substrate in this system could be regarded as the most important reason for the unacceptable performance in the adhesion test. In the case of 25L-5 (Fig. 12(d)), only a few radial cracks displaying better load capacity and further adhesion can be seen, in comparison to the previous coatings. As can be seen in Figs. 12(e, f), 25H-5 and 25M-5 exhibited great adhesion. In some regions, the pile-up of the substrate was observed, but there was no sign of delamination, spallation or cracking, thus indicating strong bonds between the layers and the substrate. The surface of these coated specimens was smooth and clean, thereby implying the good adhesion between NiP and the aluminum substrate, as well as the satisfactory adhesion between NiP and TiN coatings. This result was also in accordance with the previous findings [10,42] concerning the effect of the electroless nickel layer on the improvement of the adhesion of duplex coating systems.

6 Conclusions

(1) A quantitative method was proposed to predict the load bearing capacity of the NiP/TiN duplex coating on Al 6061 via PLS and SVR models. To overcome the problem of the small size, *K*-fold cross validation as a resampling approach was applied. The results illustrated that both models had an acceptable performance on R^2, R^2_{adj}, RMSE, AIC and BIC, but PLS was more successful than the SVR method.

(2) An equation was presented through the PLS model for load capacity in terms of three variables (thickness, adhesion and elastic modulus). All three variables were shown to have strong effects on the load bearing; however, thickness had the greatest effect.

(3) Comparison of several coated samples with various load bearing capacities confirmed the improvement in the tribological properties and adhesion behavior in terms of higher load capacity.

(4) Under a load of 2 N and during 100 m sliding, single PVD coatings were completely failed; however, for the duplex coated aluminum alloy with sufficient thickness, high adhesion and high elastic modulus, the damage was relatively small.

References

[1] LIN Song-sheng, ZHOU Ke-song, DAI Ming-jiang, FANG HU Fang, QIAN Shi, HOU Hui-jun, WEI Chun-bei, LI Fu-qiu, TONG Xin. Effects of surface roughness of substrate on properties of Ti/TiN/Zr/ZrN multilayer coatings [J]. Transactions of Nonferrous Metals Society of China, 2015, 25: 451−456.

[2] SHAN Lei, ZHANG Yang-rong, WANG Yong-xin, LI Jin-long, JIANG Xin, CHEN Jian-min. Corrosion and wear behaviors of PVD CrN and CrSiN coatings in seawater [J]. Transactions of Nonferrous Metals Society of China, 2016, 26: 175−184.

[3] LI Ze-chao, WANG Yong-xin, CHENG Xiao-ying, ZENG Zhi-xiang, LI Jin-long, LU Xia, WANG Li-ping, XUE Qun-ji. Continuously growing ultrathick CrN coating to achieve high load-bearing capacity and good tribological property [J]. ACS Applied Materials & Interfaces, 2018, 10: 2965−2975.

[4] WANG Jun-jun, PU Ji-bin, ZHANG Guan-gan, WANG Li-ping. Interface architecture for superthick carbon-based films toward low internal stress and ultrahigh load-bearing capacity [J]. ACS Applied Materials & Interfaces, 2013, 5: 5015−5024.

[5] WANG C T, HAKALA T J, LAUKKANEN A, RONKAINEN H, HOLMBERG K, GAO N, WOOD R J K, LANGDON T G. An investigation into the effect of substrate on the load-bearing capacity of thin hard coatings [J]. Journal of Materials Science, 2016, 51: 4390−4398.

[6] WARCHOLINSKI B, GILEWICZ A, KUPRIN A S, KOLODIY I V. Structure and properties of CrN coatings formed using cathodic arc evaporation in stationary system [J]. Transactions of Nonferrous Metals Society of China, 2019, 29: 799−810.

[7] KWIETNIEWSKI C, DONG H, STROHAECKER T, LI X Y, BELL T. Duplex surface treatment of high strength Timetal 550 alloy towards high load-bearing capacity [J]. Surface and Coatings Technology, 2001, 139: 284−292.

[8] BEMPORAD E, SEBASTIANI M, de FELICIS D, CARASSITI F, VALLE R, CASADEI F. Production and characterization of duplex coatings (HVOF and PVD) on Ti−6Al−4V substrate [J]. Thin Solid Films, 2006, 515: 186−194.

[9] WILSON J C A B, BANFIELD S, EICHLER J, LEYLAND A, MATTHEWS A, HOUSDEN J. An investigation into the tribological performance of physical vapour deposition (PVD) coatings on high thermal conductivity Cu-alloy substrates and the effect of an intermediate electroless Ni−P layer prior to PVD treatment [J]. Thin Solid Films, 2012, 520: 2922−2931.

[10] LIN Chung-kwei, HSU Cheng-hsun, KUNG Shu-chi. Effect of electroless nickel interlayer on wear behavior of CrN/ZrN multilayer films on Cu-alloyed ductile iron [J]. Applied Surface Science, 2013, 284: 59−65.

[11] STAIA M H, CABRERA E S, IOST A, ZAIRI A, BELAYER S, van GORP A. Tribological response of AA 2024-T3 aluminium alloy coated with a DLC duplex coating [J]. Tribology International, 2015, 85: 74−87.

[12] KOT M, RAKOWSKI W, MAJOR L, LACKNER J. Load-bearing capacity of coating–substrate systems obtained from spherical indentation tests [J]. Materials & Design, 2013, 46: 751−757.

[13] KOMVOPOULOS K. Finite element analysis of a layered elastic solid in normal contact with a rigid surface [J]. Journal of Tribology, 1988, 110(3): 477−485.

[14] ASHRAFIZADEH F. Adhesion evaluation of PVD coatings to aluminium substrate [J]. Surface and Coatings Technololgy, 2000, 130: 186−194.

[15] ZENG X T, ZHANG S, DING X Z, TEER D G. Comparison of three types of carbon composite coatings with exceptional load-bearing capacity and high wear resistance [J]. Thin Solid Films, 2002, 420/421: 366−370.

[16] KAMONCHAIVANICH K, KUBOYAMA K, OUGIZAWA T. Effect of elastic modulus and position of polyurea coating on flexural strength of coated ceramic tiles by experiments and finite element analysis [J]. Journal of Coatings Technology and Research, 2019, 16: 1201−1211.

[17] YE Yu-wei, CHEN Hao, GUO Sheng-da, SUN Shang-qi, WANG Yong-xin, ZHAO Hai-chao, WANG Li-ping. Comparison of WC/C nanocomposite films in load-bearing capacity via interface micro-cracks during tribology behavior: A feasible judgment mechanism [J]. Ceramics International, 2019, 45: 23482−23492.

[18] MILLER C, NAGY Z, SCHLUETER A. A review of unsupervised statistical learning and visual analytics techniques applied to performance analysis of non-residential buildings [J]. Renewable and Sustainable Energy Reviews, 2018, 81: 1365−1377.

[19] YAZDI M R S, KHORASANI A M, FARAJI M. Optimization of coating variables for hardness of industrial tools by using artificial neural networks [J]. Expert Systems with Applications, 2011, 38: 12116−12127.

[20] RAFIEERAD A R, BUSHROA A R, NASIRI-TABRIZI B, FALLAHPOUR A, VADIVELU J, MUSA N, KABOLI S H A. GEP-based method to formulate adhesion strength and hardness of Nb PVD coated on Ti−6Al−7Nb aimed at developing mixed oxide nanotubular arrays [J]. Journal of the Mechanical Behavior of Biomedical Materials, 2016, 61: 182−196.

[21] CHEN Tao, WU Wei-ning, LI Wen-peng, LIU De-fu. Laser cladding of nanoparticle TiC ceramic powder: Effects of process parameters on the quality characteristics of the coatings and its prediction model [J]. Optics & Laser Technology, 2019, 116: 345−355.

[22] WANG Ye, WANG Bo, ZHANG Xin-yang. A new application of the support vector regression on the construction of financial conditions index to CPI prediction [J]. Procedia Computer Science, 2012, 9: 1263−1272.

[23] ZAGHLOUL M S, HAMZA R, IORHEMEN O T, TAY J H. Comparison of adaptive neuro-fuzzy inference systems (ANFIS) and support vector regression (SVR) for data-driven modelling of aerobic granular sludge reactors [J]. Journal of Environmental Chemical Engineering, 2020, 8: 103742.

[24] WILLABY H W, COSTA D S J, BURNS B D, MACCANN C, ROBERTS R D. Testing complex models with small sample sizes: A historical overview and empirical demonstration of what Partial Least Squares (PLS) can offer differential psychology [J]. Personality and Individual Differences, 2015, 84: 73−78.

[25] FISCHER S. Surface engineering of light alloys: Aluminium, magnesium and titanium alloys [M]. Woodhead, 2016.

[26] BOUAZIZ H, BRINZA O, HADDAR N, GASPERINI M, FEKI M. In-situ SEM study of crack initiation, propagation and interfacial debonding of Ni−P coating during tensile tests: Heat treatment effect [J]. Materials Characterization, 2017, 123: 106−114.

[27] RAMALHO A, MIRANDA J C. Friction and wear of electroless NiP and NiP+ PTFE coatings [J]. Wear, 2005, 259: 828−834.

[28] SUDAGAR J, VENKATESWARLU K, LIAN J. Dry sliding wear properties of a 7075-T6 aluminum alloy coated with Ni−P (h) in different pretreatment conditions [J]. Journal of Materials Engineering and Performance, 2010, 19: 810−818.

[29] HINO M, MURAKAMI K, HIRAMATSU M, CHEN K, SAIJO A, KANADANI T. Effect of zincate treatment on adhesion of electroless Ni−P plated film for 2017 aluminum alloy [J]. Materials Transactions, 2005, 46: 2169−2175.

[30] LI Y Y, HSIAO Y C, WU C C, WU F B. Phase transformation, thermal stability and indentation behavior of sputtering Ni−P-based interlayer enhanced CrN composite coatings [J]. Surface and Coatings Technology, 2009, 204: 1002−1007.

[31] KHOR K A, GU Y W. Effects of residual stress on the performance of plasma sprayed functionally graded ZrO_2/NiCoCrAlY coatings [J]. Materials Science and Engineering A, 2000, 277: 64−76.

[32] AZADI M, ROUHAGHDAM A S. Nanomechanical properties of TiN/TiC multilayer coatings [J]. Strength of materials, 2014, 46: 121−131.

[33] ALI M, ULLAH I, NOOR W, SAJID A, BASIT A, BABER J. Predicting the session of an P2P IPTV user through support vector regression (SVR) [J]. Engineering, Technology & Applied Science Research, 2020, 10: 6021−6026.

[34] ABDI H, WILLIAMS L J. Partial least squares methods: partial least squares correlation and partial least square regression [J]. Methods in Molecular Biology, 2013, 549−579.

[35] WU Zhen-hua. Empirical modeling for processing parameters' effects on coating properties in plasma spraying process [J]. Journal of Manufacturing Processes, 2015, 19: 1−13.

[36] BI Y J, LI C, BENEZETH Y, YANG F. Impacts of multicollinearity on CAPT modalities: An heterogeneous machine learning framework for computer- assisted French phoneme pronunciation training [J]. PLoS One, 2021, 16: e0257901.

[37] REINARTZ W, HAENLEIN M, HENSELER J. An empirical comparison of the efficacy of covariance-based and variance-based SEM [J]. International Journal of Research in Marketing: A Multidisciplinary Journal, 2009, 26: 332−344.

[38] NASSER-ABU ALHIJA F, WISENBAKER J. A Monte Carlo study investigating the impact of item parceling strategies on parameter estimates and their standard errors in CFA [J]. Structural Equation Modeling: A Multidisciplinary

Journal, 2006, 13: 204−228.
[39] ALI R, RENZELLI M, KHAN M, SEBASTIANI M, BEMPORAD E. Effects of residual stress distribution on interfacial adhesion of magnetron sputtered AlN and AlN/Al nanostructured coatings on a (100) silicon substrate [J]. Nanomaterials, 2018, 8: 896.
[40] FALSAFEIN M, ASHRAFIZADEH F, KHEIRANDISH A. Influence of thickness on adhesion of nanostructured multilayer CrN/CrAlN coatings to stainless steel substrate [J]. Surfaces and Interfaces, 2018, 13: 178−185.
[41] HUANG Biao, ZHOU Qiong, ZHANG Er-geng. Effect of thickness on tribological behavior of hydrogen free diamond-like carbon coating [J]. Coatings, 2020, 10: 243.
[42] HSU Cheng-hsun, CHEN Kai-lin, LU Jia-hong. Effects of electroless nickel interlayer on surface properties of CrN arc-coated austempered ductile iron [J]. Surface and Coatings Technology, 2008, 203: 868−871.
[43] LIEW K W, KONG H J, LOW K O, KOK C K, LEE D. The effect of heat treatment duration on mechanical and tribological characteristics of Ni–P–PTFE coating on low carbon high tensile steel [J]. Materials & Design (1980—2015), 2014, 62: 430−442.
[44] AHMADKHANIHA D, ERIKSSON F, LEISNER P, ZANELLA C. Effect of SiC particle size and heat-treatment on microhardness and corrosion resistance of NiP electrodeposited coatings [J]. Journal of Alloys and Compounds, 2018, 769: 1080−1087.
[45] AWAD S H, QIAN H C. Deposition of duplex Al_2O_3/TiN coatings on aluminum alloys for tribological applications using a combined microplasma oxidation (MPO) and arc ion plating (AIP) [J]. Wear, 2006, 260: 215−222.
[46] QU J, XU H B, FENG Z L, FREDERICK D A, AN L N, HEINRICH H. Improving the tribological characteristics of aluminum 6061 alloy by surface compositing with sub-micro-size ceramic particles via friction stir processing [J]. Wear, 2011, 271: 1940−1945.
[47] AL-QUTUB A M, KHALIL A, SAHEB N, HAKEEM A. Wear and friction behavior of Al6061 alloy reinforced with carbon nanotubes [J]. Wear, 2013, 297: 752−761.
[48] RAMESH C S, KESHAVAMURTHY R, CHANNABASAPPA B H, PRAMOD S. Friction and wear behavior of Ni−P coated Si_3N_4 reinforced Al6061 composites [J]. Tribology international, 2010, 43: 623−634.
[49] ALLAHYARZADEH M H, ALIOFKHAZRAEI M, ROUH AGHDAM A S, ALIMADADI H, TORABINEJAD V. Mechanical properties and load bearing capability of nanocrystalline nickel−tungsten multilayered coatings [J]. Surface and Coatings Technology, 2020, 386: 125472.
[50] ANVARI S R, MONIRVAGHEFI S M, ENAYATI M H. Wear characteristics of functionally graded nanocrystalline Ni−P coatings [J]. Surface Engineering, 2015, 31: 693−700.
[51] OTHMAN I, STARINK M, WANG S C. Impact of single and double zincating treatment on adhesion of electrodeposited nickel coating on aluminium alloy 7075 [J]. Journal of Advanced Manufacturing Technology, 2018, 12: 179−192.
[52] FRANCO M, SHA W, ALDIC G, MALINOV S, ÇIMENOĞLU H. Effect of reinforcement and heat treatment on elevated temperature sliding of electroless Ni−P/SiC composite coatings [J]. Tribology International, 2016, 97: 265−271.
[53] MITTAL K L. Adhesion aspects of thin films: Volume 1 [M]. Zeist, The Netherlands: Vsp, 2001.
[54] KHLIFI K, BEN CHEIKH LARBI A. Investigation of adhesion of PVD coatings using various approaches [J]. Surface Engineering, 2013, 29: 555−560.

基于 PLS 和 SVR 模型评价铝合金双层涂层承载能力的新方法

Farideh DAVOODI[1], Fakhreddin ASHRAFIZADEH[1], Masoud ATAPOUR[1], Reyhaneh RIKHTEHGARAN[2]

1. Department of Materials Engineering, Isfahan University of Technology, Isfahan 84156-83111, Iran;
2. Department of Mathematical Sciences, Isfahan University of Technology, Isfahan 84156-83111, Iran

摘　要：为提高铝合金的承载能力，在 AA6061 铝合金表面制备由化学镀中间层和物理气相沉积(PVD)表面层组成的双层 NiP/TiN 涂层。根据涂层的厚度、附着力和弹性模量，采用偏最小二乘法(PLS)和支持向量回归(SVR)法模拟涂层的承载。结果表明，两种模型均可以模拟涂层的承载，但 PLS 模型优于 SVR 模型。厚度、附着力和弹性模量与载荷的相关系数分别为 0.841、0.8092 和 0.7657，可见厚度对承载能力的影响最大。用 XRD 和 SEM 对样品的组成和结构进行表征，通过对涂层的磨损和附着力的评价，讨论涂层的承载能力。在 2 N 载荷和 100 m 滑动距离下的干滑动磨损试验表明，涂层试样在低荷载作用下被完全破坏。Rockwell 表面硬度测试表明，具有高承载能力的样品不仅具有优良的摩擦学性能，还具有更大的附着力。

关键词：承载；铝合金；NiP 夹层；TiN 涂层；偏最小二乘法；支持向量回归

(Edited by Xiang-qun LI)